Chinese Chemical Letters 31 (2020) 2045–2049

Contents lists available at ScienceDirect

Chinese Chemical Letters

journal homepage: www.elsevier.com/locate/cclet

Communication

High performance ethylene sensor based on palladium-loaded tin oxide: Application in fruit quality detection

Qiuni Zhao[a], Zaihua Duan[a], Zhen Yuan[a], Xian Li[b], Si Wang[a], Bohao Liu[a], Yajie Zhang[a], Yadong Jiang[a], Huiling Tai[a,*]

[a] State Key Laboratory of Electronic Thin Films and Integrated Devices, School of Optoelectronic Science and Engineering, University of Electronic Science and Technology of China (UESTC), Chengdu 610054, China
[b] Agricultural Information Institute, Chinese Academy of Agricultural Sciences, Key Laboratory of Agricultural Information Service Technology of Ministry of Agriculture, Beijing 100081, China

ARTICLE INFO

Article history:
Received 13 January 2020
Received in revised form 17 February 2020
Accepted 18 February 2020
Available online 1 May 2020

Keywords:
Ethylene sensing
Pd-loaded SnO_2
High performance
Low detection limit
Fruit quality monitoring

ABSTRACT

Ethylene (C_2H_4), as a plant hormone, its emission can be served as an indicator to measure fruit quality. Due to the limited physiochemical reactivity of C_2H_4, it is a challenge to develop high performance C_2H_4 sensors for fruit detection. Herein, this paper presents a resistive-type C_2H_4 sensor based on Pd-loaded tin oxide (SnO_2). The C_2H_4 sensing performance of proposed sensor are tested at optimum operating temperature (250 °C) with ambient relative humidity (51.9% RH). The results show that the response of Pd-loaded SnO_2 sensor (11.1, R_a/R_g) is about 3 times higher than that of pristine SnO_2 (3.5) for 100 ppm C_2H_4. The response time is also significantly shortened from 7 s to 1 s compared with pristine SnO_2. Especially, the Pd-loaded SnO_2 sensor possesses good sensitivity (0.58 ppm^{-1}) at low concentration (0.05–1 ppm) with excellent linearity (R^2 = 0.9963) and low detection limit (50 ppb). The high sensing performance of Pd-loaded SnO_2 are attributed to the excellent adsorption and catalysis effects of Pd nanoparticle. Meaningfully, the potential applications of C_2H_4 sensor are performed for monitoring the maturity and freshness of fruits, which presents a promising prospect in fruit quality evaluation.

Ethylene (C_2H_4) as a colorless and odorless phytohormone is closely related to the maturity and freshness of fruit [1]. For example, low concentration of C_2H_4 (from 10 ppb to 10 ppm) would be released from immature fruit, and C_2H_4 also triggers ripening genes resulting in changes in texture, color and taste of fruit [2]. With the fruit maturing, the C_2H_4 production increases gradually to over 100 ppm. Thus, the emission of C_2H_4 can be used as an indicator of fruit maturity [3]. Furthermore, excess C_2H_4 during fruit storage can accelerate respiratory rates of fruits resulting in senescence and even spoilage [4]. Therefore, in order to evaluate the quality of fruit efficiently and intelligently, it is important to develop a high performance gas sensor for detecting C_2H_4 concentration at trace level.

Up to now, various techniques, including optical, electrical and mass-sensitive methods, have been applied for C_2H_4 detection. Among them, gas chromatography [5], fluorescence [6], photo-acoustic spectroscopy [7] could achieve high-sensitive detection of C_2H_4, but the expensive cost, bulky and non-portability of these methods largely impede their application in fruit detection. Instead, the resistive-type sensor are worth exploring because of its simple and affordable. Due to the limited physiochemical reactivity of C_2H_4, C_2H_4 sensors working at room temperature have poor performance [8–11]. In order to accelerate the adsorption and desorption of nonpolar C_2H_4 molecules on sensitive materials, it is necessary to use assistant methods such as heating [12] or ultraviolet irradiation [13]. Several C_2H_4 sensors based on heating have been reported in the literature [14–20]. For example, Kathirvelan *et al.* studied the C_2H_4 sensing properties of titanium dioxide and tungsten trioxide (TiO_2-WO_3) nanocomposites at 250 °C, the minimum achievable concentration was 8 ppm for continuous detection and the response time is unknown [14]. Nimittrakoolchai *et al.* reported a WO_3 gas sensor prepared by precipitation method, the detection range is 3–10 ppm and the response time is about a few minutes for 3–5 ppm C_2H_4 [15]. Wang *et al.* employed a porous zinc oxide (ZnO) nanosheets based C_2H_4 gas sensor, it is of 5 ppm detection limit and the response less than 2 at 500 °C [16]. Progress has been made in resistive-type C_2H_4 sensors, but the detection limit, response value and response time still need to be improved.

* Corresponding author.
E-mail address: taitai1980@uestc.edu.cn (H. Tai).

https://doi.org/10.1016/j.cclet.2020.04.032
1001-8417/

In order to enhance the performance of gas sensor, using noble metals (*e.g.*, Pt [17], Au [21], Ag [22] and Pd [23]) loaded metal oxide semiconductors (MOS) is a prevalent strategy. In particular, as a potential C_2H_4 acceptor and catalyst [24–26], Pd loaded MOS is expected to achieve high response, fast speed and low detection limit. Herein, Pd-loaded tin oxide (SnO_2) is used to prepare C_2H_4 gas sensor. The C_2H_4 sensing properties are investigated at 50–400 °C, and the C_2H_4 gas sensing mechanism is discussed in this paper. Particularly, the potential application of Pd-loaded SnO_2 C_2H_4 sensor has been developed in fruit detection.

The Pd-loaded SnO_2 C_2H_4 sensor (Fig. S1a in Supporting information) was fabricated by simple coating method, and the details referred to the supplementary material. The micro-morphologies, lattice images, crystallization and chemical valence states of pristine SnO_2 and Pd-loaded SnO_2 were characterized by various techniques including scanning electron microscopy (SEM, Zeiss, SUPRA 55), transmission electron microscope (TEM, FEI, Tecnai G2 F20 S-TWIN), X-ray diffraction (XRD, Bruker, D8 Advance) with a range of 2θ from 20° to 80° at 40 kV and 40 mA using Co-Kα as the irradiation source (λ = 0.1789 nm), and X-ray photoelectron spectroscopy (XPS, Thermo Fisher Scientific, K-Alpha), respectively.

The C_2H_4 sensing performance of sensors were measured by a dynamic homemade system with the Keithley 2700 data acquisition instrument and a regulated power supply (Fig. S1b in Supporting information). The operating temperature of sensor was varied between 50 °C and 400 °C. In order to simulate the conventional atmospheric environment, the testing relative humidity (RH) is controlled at 51.9% by air with bubbling distilled water [27,28], and calibrated by a high-accuracy hygrometer (CEM, DT-625, Shenzhen Everbest Machinery Industry Co., Ltd., China). The response of gas sensor is calculated as following equation: Response = R_a/R_g (R_a: resistance under the air, R_g: resistance under the target gas). The sensitivity is defined as the slope of response–concentration linear fitting curve. And the response/recovery times are defined as the time taken by C_2H_4 gas sensor to achieve 90% of the total resistance change in the case of adsorption and desorption respectively.

The SEM images of pristine SnO_2 and Pd-loaded SnO_2 are shown in Fig. S2 (Supporting information). It can be seen that both of them are composed of nanoparticles, but there is no obvious difference in microscopic morphology of two SEM images. In order to confirm the existence of Pd, the XRD patterns of pristine SnO_2 and Pd-loaded SnO_2 are characterized in Fig. 1a. All the diffraction peaks of SnO_2 can be well coincided with JCPDS card No. 41-1445 and match the tetragonal rutile structure [29], the diffraction peaks of Pd are tally with JCPDS data No. 46-1043, which reflect the face-centered cubic crystalline structure [30]. Compared with the prominent peaks of SnO_2, the weak diffraction peaks of Pd indicate that the trace existence of Pd in composite film. The TEM images of Pd-loaded SnO_2 are performed as shown in Figs. 1b and c. The lattice fringes with an inter-planar distance of 0.33 nm coincide well with the (110) plane of SnO_2 in Fig. 1c. And the lattice distance of 0.22 nm is correspond to the (111) crystalline plane of Pd, which further suggests that the Pd-loaded SnO_2 nanoparticles have been successfully synthesized from the micro-morphology. It is beneficial to regulate the interface barrier between SnO_2 and Pd [31].

The surface compositions and chemical valence states are analyzed by XPS. Fig. 1d is the full range XPS spectra of pristine SnO_2 and Pd-loaded SnO_2. Fig. 1e displays the O 1s spectra of SnO_2 and the binding energies at 530.2, 531.5 and 533.3 eV can be assigned to lattice oxygen species (O_L), oxygen vacancy (O_V) and the chemisorbed oxygen species (O_C, H_2O species and impurity oxygen) on the surface of sensing materials, respectively [32–34]. The oxygen vacancy has significant influence on the gas sensing properties of resistance-type MOS [33]. Compared Fig. 1f with Fig. 1e, the content of oxygen vacancy in Pd-loaded SnO_2 (40.3%) is higher than pristine SnO_2 (30.6%). The increase of oxygen vacancies of Pd-loaded SnO_2 is conducive to C_2H_4 reaction and further enhance the sensing performance [34]. The higher content of chemisorbed oxygen (15.3%) in pristine SnO_2 could be due to the adsorption of water molecules [35,36]. The high-resolution XPS spectra of Pd 3d is shown in Fig. S3 (Supporting information), the Pd $3d_{5/2}$ electron binding energies in palladium oxide (PdO) and metallic Pd are 335.9 and 334.5 eV, respectively [31]. The contents of PdO of Pd-loaded SnO_2 are calculated to be 58%, it is confirmed

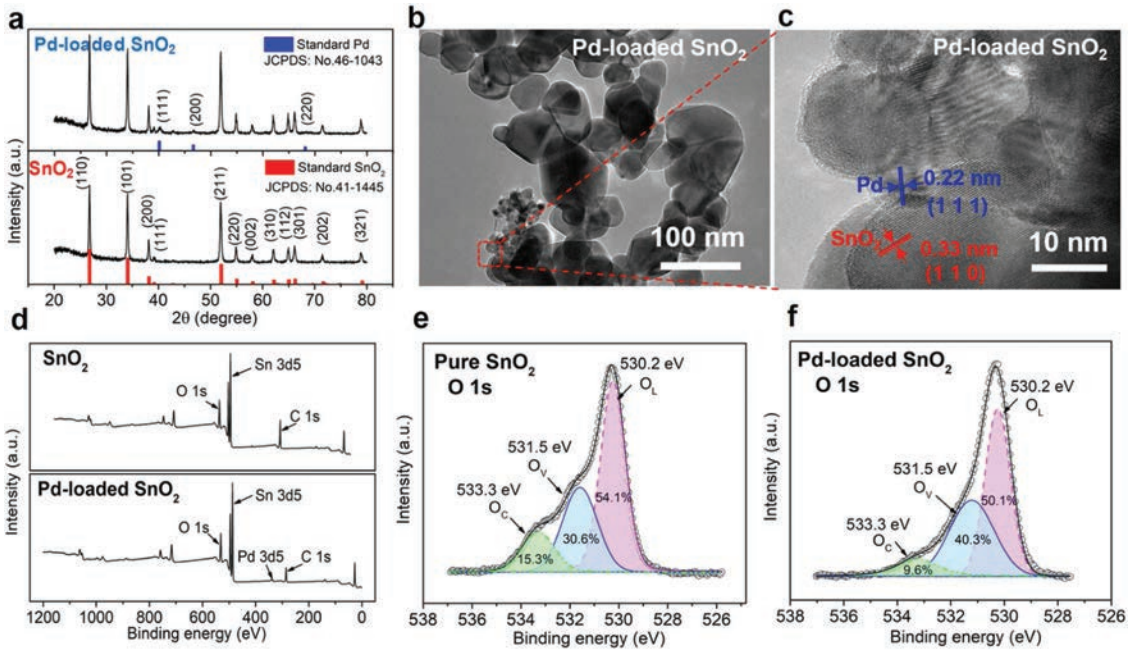

Fig. 1. (a) XRD patterns of pristine SnO_2 and Pd-loaded SnO_2. (b) TEM image of Pd-loaded SnO_2. (c) HRTEM image of Pd-loaded SnO_2. (d) XPS fully scanned spectra. XPS spectra: O 1s spectra of (e) pristine SnO_2 and (f) Pd-loaded SnO_2.

that Pd nanoparticles are easy to oxidize into PdO in air due to their strong electron transport ability. Moreover, the conversion of Pd and PdO in the oxygen environment plays an important role in MOS sensitization [24].

The working temperature has great influence on the response of MOS based gas sensors [37]. In order to investigate the relationship between operating temperature and the C_2H_4 sensing properties, the response of sensors based on pristine SnO_2 and Pd-loaded SnO_2 to 10 ppm C_2H_4 at operating temperatures ranging from 50 °C to 400 °C are shown in Fig. 2a. As can be seen, the addition of Pd reduces the optimum working temperature of gas sensor from 350 °C to 250 °C. The phenomena of the increasing sensing response and the decreasing working temperature for SnO_2 are consistent with the previous researches by Zhang's group [38], which directly verifies the promotion effect of Pd nanoparticles. Fig. 2b displays the real-time resistance variation curves of two gas sensors to 20–100 ppm C_2H_4 at 250 °C. When exposed to 100 ppm C_2H_4, the response of Pd-loaded SnO_2 sensor (11.1) is about 3 times higher than that of pristine SnO_2 (3.5). Moreover, the response time is also significantly shortened from 7 s to 1 s compared with pristine SnO_2. As shown in Fig. 2c, both of two sensors exhibit good linearity, but the Pd-loaded SnO_2 gas sensor holds a larger sensitivity (0.05 ppm^{-1}) than that of pristine SnO_2 one (0.02 ppm^{-1}). Fig. 2d displays the linear fitting curves of two sensors to low concentration C_2H_4 (0.05–1 ppm), the Pd-loaded SnO_2 gas sensor exhibits better sensitivity (0.58 ppm^{-1}) with excellent linearity (R^2 = 0.9963). Especially, the Pd-loaded SnO_2 gas sensor achieves ultra-low detection concentration (50 ppb) (the inset of Fig. 2d). The real-time resistance variation curves of two sensors corresponding to Fig. 2d are shown in Figs. S4 and S5 (Supporting information). Fig. 2e exhibits the response and recovery curves for three cycles when the Pd-loaded SnO_2 gas sensor is exposed to 100 ppb, 1 ppm and 40 ppm C_2H_4 concentrations. As can be seen, the response and recovery curves can switch to the steady states after the C_2H_4 level changed, indicating that the sensor shows good repeatability in the continuous measurements. Fig. 2f presents the good stability and durability of the Pd-loaded SnO_2 gas sensor for low concentration C_2H_4 in a week. Moreover, the other sensing performance (humidity, selectivity) of Pd-loaded SnO_2 gas sensor are studied in supplementary material. Compared with previous works [8–11,14–20], the C_2H_4 sensor based on Pd-loaded SnO_2 shows high performance in terms of the response value (R_a/R_g = 11.1 for 100 ppm), detection limit (≤50 ppb) and response speed (1 s for 100 ppm), which are listed detailly in Table 1.

A plausible explanation of C_2H_4 sensing mechanism for Pd-loaded SnO_2 sensor is discussed as follows. As shown in Fig. 3a, since the work function of Pd (5.12 eV) is higher than that of SnO_2 (4.5 eV), the Schottky junction will be formed at the interface of Pd and SnO_2, which causes the part of electrons transfer from SnO_2 to Pd [39]. It is beneficial to the formation of depletion region around SnO_2. When the Pd-loaded SnO_2 gas sensor is exposed to air (Fig. 3b), oxygen molecules combine with electrons to form adsorbed oxygen (O^- at 250 °C) on the surface area of Pd-loaded SnO_2, resulting in a thick electron-depleted layer [40]. Furthermore, Pd (PdO) as a catalyst activates the dissociation of oxygen molecules and enhances the adsorption activity of oxygen on the surface of SnO_2 [41]. The increase of oxygen vacancy of Pd-loaded SnO_2 is also proved by XPS analysis. The thicker electron-depleted layer results in the increase of air resistance of SnO_2 after Pd loading [24], which is beneficial to improve the C_2H_4 sensing response of SnO_2 sensor.

When the Pd-loaded SnO_2 gas sensor is exposed to C_2H_4 gas (Fig. 3c), C_2H_4 molecules with a carbon-carbon double bond (C = C) are oxidized to ethylene oxide or acetaldehyde, then further reacted to produce carbon dioxide (CO_2) and water (H_2O), and the reaction process can be shown as follows [42]:

$$C_2H_{4(ads)} + O^-_{(ads)} \rightarrow C_2H_4O + e^- \quad (1)$$

$$C_2H_4O + 5O^-_{(ads)} \rightarrow 2CO_2 + 2H_2O + 5e^- \quad (2)$$

The process of C_2H_4 oxidation releases the trapped electrons back to the conduction band, leading to the reduction of depletion region and the decrease in resistance. As the potential receptors of

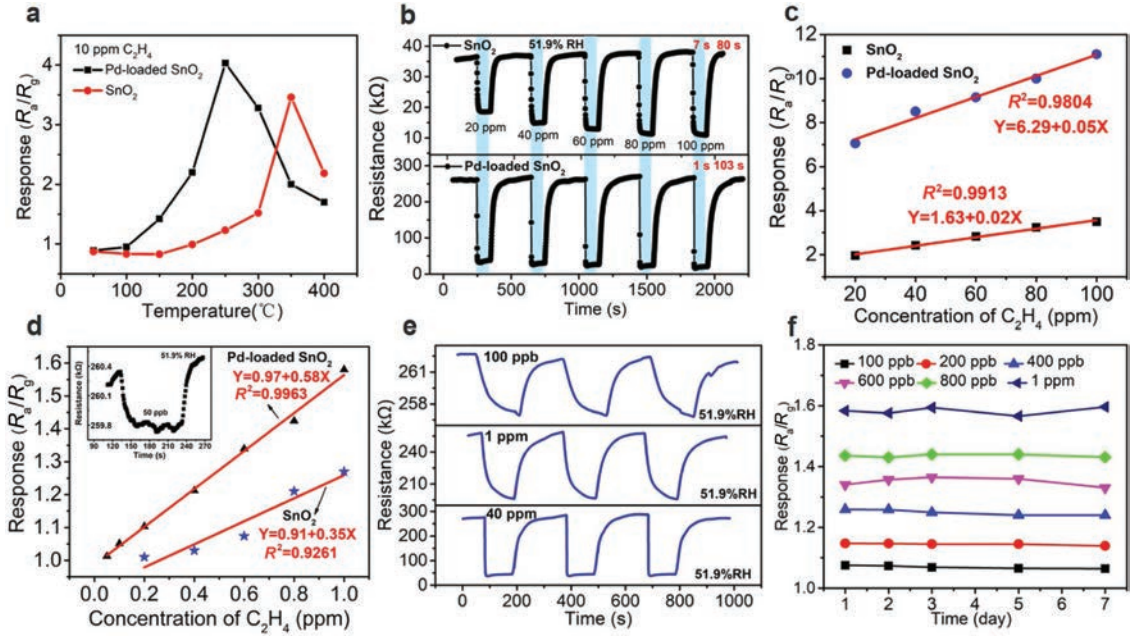

Fig. 2. (a) Response of the pristine SnO_2 and Pd-loaded SnO_2 sensors to 10 ppm C_2H_4 at different working temperature. (b) Real-time resistance variation curves and (c) linear fitting curves of response for pristine SnO_2 and Pd-loaded SnO_2 sensors to 20–100 ppm C_2H_4 at 250 °C. (d) Linear fitting curves of response to 0.05–1 ppm C_2H_4 at 250 °C, the inset of (d) is the resistance variation curves to 50 ppb C_2H_4. (e) Repeatability curves. (f) Stability curves in a week.

Table 1
Gas sensing properties of reported resistive-type C_2H_4 gas sensors.

Materials	Response (R_a/R_g)	Detection limit	Response time (s)	Temperature (°C)	References
SWNTs/copper(I) complex	<2 (50 ppm)	500 ppb	–	r.t.	[8]
PNAI-H_2SO_4	1.25 (100 ppm)	10 ppm	–	r.t.	[9]
MWCNTs	< 2 (100 ppm)	10 ppm	10	r.t.	[10]
PANI/MWCNTs/SnO_2	~1.2 (100 ppm)	10 ppm	–	r.t.	[11]
TiO_2-WO_3	~1.25 (100 ppm)	8 ppm	–	250	[14]
WO_3	1.1 (3 ppm)	3 ppm	>60	300	[15]
Porous ZnO	< 2 (100 ppm)	5 ppm	8	500	[16]
SnO_2-1% Pt	3.16 (100 ppm)	1 ppm	–	250	[17]
Silicalite-1/ SnO_2	~3.9 (70 ppm)	8 ppm	14	350	[18]
SnO_2	10.43 (100 ppm)	10 ppm	270	300	[19]
WO_3	~2 (200 ppm)	200 ppm	~67	350	[20]
SnO_2	5 (200 ppm)	200 ppm	~83	350	[20]
Pd-SnO_2	11.1 (100 ppm)	50 ppb	1	250	This work

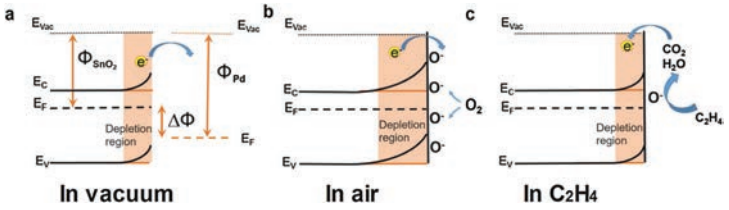

Fig. 3. Schematic diagram of C_2H_4 sensing mechanism for Pd-loaded SnO_2 gas sensor. Schottky barrier in (a) vacuum, (b) air and (c) C_2H_4.

C_2H_4, Pd nanoparticles can increase the number of efficient adsorption sites of C_2H_4 molecules near the surface of sensitive film [26]. Moreover, adsorbed C_2H_4 molecules on Pd will spillover onto the surface of SnO_2 because of the spillover effect [43], leading to the high sensing response. In summary, the C_2H_4 gas-sensing mechanism of Pd-loaded SnO_2 can be explained by depletion layer theory, the catalysis and receptor function of Pd.

The C_2H_4 emission can be used as an indicator to estimate the coloration, texture, and flavor taste of fruits [44]. Inspired by the demand for fruit freshness and ripeness monitoring, potential applications of Pd-loaded SnO_2 gas sensor are explored. The temperature and humidity of the laboratory are controlled at 25 ± 2 °C and $50\% \pm 5\%$ RH by an air conditioner, and recorded by the high-accuracy hygrometer. Fig. 4 displays the response curves in the application of fruit quality detection. In order to simulate the storage conditions and observe morphological changes, fruits are put into a transparent bottle packed with porous plastic wrap to avoid fermentation, and then place the gas sensor at the bottle mouth during detection. Fig. 4a shows the real-time response curves of the gas sensor to four fresh fruits (banana, lemon, apple and pear), the weight of each fruit is about 120–150 g. It can be seen that the Pd-loaded SnO_2 gas sensor presents different responses to different fruits. Fig. 4b displays the increasing response to gradually increasing banana weight (about 25 g, 50 g, 75 g, 100 g and 125 g). The nonlinear increase indicates that C_2H_4 emissions are mutually reinforcing [2]. To further support potential applications in fruit storage, Fig. 4c presents the variation in response to one banana at different ripening stages. As a comparison, the same test to lemon is shown in Fig. 4d. The results show that the response of banana changed significantly from non-climacteric to climacteric, while that of lemon changed smoothly. As a respiratory climacteric fruit, banana is susceptible to the influence of C_2H_4 concentration in senescence and metamorphosis, while the non-respiration climacteric lemon is more resistant to storage than banana due to the slow metabolism of lemon, which is consistent with the experimental results. In short, the above tests demonstrate that different species, quantities and storage states of fruits can be estimated by the Pd-loaded SnO_2 gas sensor like a smart nose, which suggest that the potential applications of Pd-loaded SnO_2 gas sensor in fruits quality evaluation.

In summary, a Pd-loaded SnO_2 C_2H_4 sensor for fruit quality evaluation is fabricated by coating method. The high sensing performance of Pd-loaded SnO_2 C_2H_4 sensor are obtained at 250 °C, it is of high response (11.1 for 100 ppm), fast speed (1 s for 100 ppm), good linearity (R^2 = 0.9804 for 20-100 ppm), low detection limit (50 ppb) and good stability. The sensing mechanism of Pd-loaded SnO_2 sensor is discussed by the depletion layer theory, the catalysis and receptor function of Pd. Furthermore, the applications of the Pd-loaded SnO_2 sensor in detecting fruit species, quantities and storage states are explored. The results show that

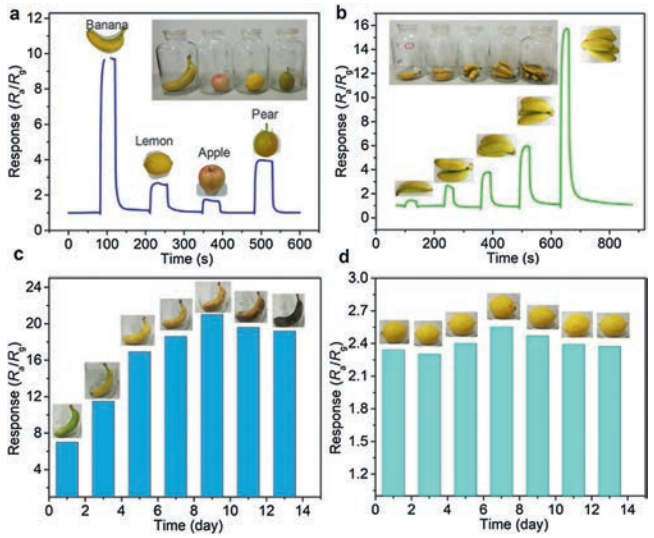

Fig. 4. Potential applications of the Pd-loaded SnO_2 gas sensor: real-time response curves to (a) various fruits, (b) bananas with different quantities, (c) one banana in half a month, (d) one lemon in half a month.

the prepared Pd-loaded SnO_2 sensor has great potential for developing high-performance C_2H_4 sensor in fruit quality monitoring.

Declaration of competing interest

The authors declare that they have no known competing financial interests or personal relationships that could have appeared to influence the work reported in this paper.

Acknowledgments

This work is supported by the National Science Funds for Excellent Young Scholars of China (No. 61822106), National Science Funds for Creative Research Groups of China (No. 61421002), Natural Science Foundation of China (No. 61671115) and Central Public-interest Scientific Institution Basal Research Fund (No. Y2019XK18).

Appendix A. Supplementary data

Supplementary material related to this article can be found, in the online version, at doi:https://doi.org/10.1016/j.cclet.2020.04.032.

References

[1] F. Mustafa, S. Andreescu, Foods 7 (2018) 168.
[2] C.S. Barry, J.J. Giovannoni, J. Plant Growth Regul. 26 (2007) 143.
[3] F. Caprioli, L. Quercia, Sens. Actuator. B -Chem. 203 (2014) 187–196.
[4] S. Janssen, K. Schmitt, M. Blanke, et al., Phil. Trans. R. Soc. 372 (2014) 20130311.
[5] N.A. Zaidi, M.W. Tahir, M.J. Vellekoop, W. Lang, Sensors 18 (2018) 2589.
[6] M. Sun, X. Yang, Y. Zhang, et al., J. Agric. Food Chem. 67 (2019) 507–513.
[7] Y. Hitomi, T. Nagai, M. Kodera, Chem. Commun. 48 (2012) 10392–10394.
[8] B. Esser, J.M. Schnorr, T.M. Swager, Angew. Chem. Int. Ed. 51 (2012) 5752–5756.
[9] P. Pattananuwat, D. Aht-Ong, Mater. Sci. Forum 654-656 (2010) 2285–2288.
[10] J. Kathirvelan, R. Vijayaraghavan, J. Sensors 2014 (2014) 6.
[11] P. Pattananuwat, D. Aht-Ong, Polymer-Plast. Tech. 52 (2013) 189–194.
[12] C. Yang, Y. Xu, L. Zheng, et al., Chin. Chem. Lett. (2020), doi:http://dx.doi.org/10.1016/j.cclet.2020.01.011.
[13] Y. Li, D.L. Li, J.C. Liu, Chin. Chem. Lett. 26 (2015) 304–308.
[14] J. Kathirvelan, Sensor Rev. 37 (2017) 147–154.
[15] O.U. Nimittrakoolchai, S. Supothina, Mater. Chem. Phys. 112 (2008) 270–274.
[16] L.P. Wang, Z. Jin, T. Luo, et al., New J. Chem. 43 (2019) 3619–3624.
[17] P. Ivanov, E. Llobet, A. Vergara, et al., Sens. Actuator. B -Chem. 111-112 (2005) 63–70.
[18] D. Jadsadapattarakul, C. Thanachayanont, J. Nukeaw, T. Sooknoi, Sens. Actuator. B -Chem. 144 (2010) 73–80.
[19] H. Ahn, J.H. Noh, S.B. Kim, et al., Mater. Chem. Phys. 124 (2010) 563–568.
[20] M. Krivec, R. Leitner, R. Waldner, J. Gostner, F. Überall, SPIE2015 205 (2020) 951713.
[21] L. Liang, J. Yin, J. Bao, et al., Chin. Chem. Lett. 30 (2019) 167–170.
[22] J. Zhang, X. Liu, G. Neri, N. Pinna, Adv. Mater. 28 (2016) 795–831.
[23] D. Amalric-Popescu, F. Bozon-Verduraz, Catal. Today 70 (2001) 139–154.
[24] G. Li, X. Wang, L. Yan, et al., ACS Appl. Mater. Interfaces 11 (2019) 26116–26126.
[25] H. Li, J. Xu, Y. Zhu, X. Chen, Q. Xiang, Talanta 82 (2010) 458–463.
[26] K. Besar, J. Dailey, H.E. Katz, ACS Appl. Mater. Interfaces 9 (2017) 1173–1177.
[27] Q. Zhao, Z. Yuan, Z. Duan, et al., Sens. Actuator. B -Chem. 289 (2019) 182–185.
[28] Z. Duan, Y. Jiang, M. Yan, et al., ACS Appl. Mater. Interfaces 11 (2019) 21840–21849.
[29] Z. Zhang, Y. Hou, S. Zhang, et al., Chin. Chem. Lett. 29 (2018) 1656–1660.
[30] Y. Li, L. Wang, J. Low, et al., Chin. Chem. Lett. 31 (2020) 231–234.
[31] D.J. Yang, I. Kamienchick, D.Y. Youn, A. Rothschild, I.D. Kim, Adv. Funct. Mater. 20 (2010) 4258–4264.
[32] H. Wang, L. Zhou, Y. Liu, et al., Sens. Actuator. B -Chem. 305 (2020) 127498.
[33] Y. Zhang, D. Li, L. Qin, et al., Sens. Actuator. B -Chem. 255 (2018) 2240–2247.
[34] S. Semancik, T.B. Fryberger, Sens. Actuator. B -Chem. 1 (1990) 97–102.
[35] J.L.G. Fierro, Catal. Today 8 (1990) 153–174.
[36] Z. Yang, Z. Zhang, K. Liu, Q. Yuan, B. Dong, J. Mater. Chem. C 3 (2015) 6701–6708.
[37] T. Zhao, Y. Ren, G. Jia, et al., Chin. Chem. Lett. 30 (2019) 2032–2038.
[38] L. Wang, H. Dou, Z. Lou, T. Zhang, Nanoscale 5 (2013) 2686–2691.
[39] F. Li, T. Zhang, X. Gao, R. Wang, B. Li, Sens. Actuator. B -Chem. 252 (2017) 822–830.
[40] L. Qiao, Y. Bing, Y. Wang, et al., Sens. Actuator. B -Chem. 241 (2017) 1121–1129.
[41] D. Haridas, V. Gupta, Sens. Actuator. B -Chem. 166 (2012) 156–164.
[42] M. Agarwal, M.D. Balachandran, S. Shrestha, K. Varahramyan, J. Nanomater. 2012 (2012) 5.
[43] K. Tomishige, Y. Nakagawa, M. Tamura, Chin. Chem. Lett. 31 (2020) 1071–1077.
[44] C.S. Günther, K.B. Marsh, R.A. Winz, et al., Food Chem. 169 (2015) 5–12.